The/1sO record of Globigerinoides ruber (white)

L. Wang, M. Sarnthein, J.-C. Duplessy, H. Erlenkeuser, S. Jung, U. Pflaumann

PALEOCEANOGRAPHY, VOL. 10, NO. 4, PAGES 749-761, AUGUST 1995

Paleo sea surface salinities in the low-latitude Atlantic: The $\delta^{18}O$ record of *Globigerinoides ruber* (white)

L. Wang,[1] M. Sarnthein,[1] J-C. Duplessy,[2] H. Erlenkeuser,[3] S. Jung,[1] and U. Pflaumann[1]

Abstract. On the basis of the comparison of $\delta^{18}O$ values of *Globigerinoides ruber* (white) ($\delta^{18}O_{G.\,ruber}$) from modern sediments and measured sea surface temperatures (SST) and salinity (SSS), $\delta^{18}O_{G.\,ruber}$ values most clearly record summer SST and SSS of the uppermost 50 m of water in the low-latitude Atlantic. A new transfer equation is presented for estimating local summer paleo SSS at 0-50 m depth using $\delta^{18}O_{G.\,ruber}$, paleo SST, and the global $\delta^{18}O$ ice effect of sea water, with the standard error reaching ±0.72 - ±0.77‰ SSS. The equation was applied to a 35 kyr long $\delta^{18}O_{G.\,ruber}$ record and paleo SST estimates based on planktonic foraminiferal assemblages to reconstruct the paleo SSS changes along the east Atlantic margin off the northwest Sahara. The resulting local SSS show a general increase by 0.3-1.4‰ during the last glacial maximum (LGM) and large parts of glacial Termination I, suggesting a general increase in the upwelling of the highly saline North Atlantic Central Water and/or a reduced lateral advection of less saline Canary Current water. Two short salinity lows (up to 0.35‰ less than today) during and after the LGM are coeval with the Heinrich meltwater events 1 and 2 in the North Atlantic, indicating the breakdown of coastal upwelling and meltwater advection from the north. Both events are followed by an extreme SSS maximum (38.15‰) along with the restoration of the salinity conveyor belt. At 9.0-5.5 ka the salinity minimum (up to 0.65‰ less than today) reflects the continental runoff linked to the phase of strong North Saharan humidity during the early Holocene climatic optimum.

Introduction

Recent paleo salinity reconstructions from $\delta^{18}O$ values of planktonic foraminifera in the high-latitude and midlatitude North Atlantic and the equatorial Indian Ocean show that the distribution of sea surface salinity (SSS) has markedly differed from today during the last glacial maximum (LGM) [*Duplessy et al.*, 1991, 1993; *Rosteck et al.*, 1993]. Variations in SSS and sea surface temperature (SST) in both low and high latitudes during the LGM suggest a systematic change in the global thermohaline circulation. In order to better understand these variations in the global oceanic salt budget, the reconstruction of surface salinity in the low-latitude Atlantic is of special interest, because it may provide important insights into various underlying climatic processes such as (1) evaporation from and (2) precipitation over the ocean. (3) Near the continental margin, it may help reconstructing the freshwater input from the subtropical continents, both as a result and record of changes in continental aridity/humidity.

[1]Geologisch-Paläontologisches Institut, Universität Kiel, Kiel, Germany

[2]Centre des Faibles Radioactivités, Laboratoire mixte CNRS-CEA, Gif-sur-Yvette Cedex, France

[3]C14-Labor, Institut für Reine und Angewandte Kernphysik, Universität Kiel, Kiel, Germany

Paper number 95PA00577.
0883-8305/95/95PA-00577$10.00

The planktonic foraminifera *Globigerinoides ruber* (white) lives and calcifies in the topmost surface layer of the ocean (0-25 m) [*Tolderlund and Bé*, 1971; *Fairbanks et al.*, 1982; *Williams et al.*, 1981; *Hemleben et al.*, 1989]. Hence the shell composition of this species is a good candidate to be used for estimating paleo SSS in a low-latitude ocean. In this paper, we present a strategy to calibrate the oxygen isotope values of calcite tests of *G. ruber* (white) with the modern SSS and SST distribution. Moreover, we test this relationship with a downcore record from the low-latitude eastern Atlantic using paleo SST data derived from planktonic foraminifera assemblages [U. Pflaumann et al. SIMMAX, a transfer technique to deduce sea surface temperature from planktonic foraminifera - the EPOCH approach submitted to Paleoceanography, 1995; hereinafter referred to as Pflaumann et al., submitted manuscript; also Pflaumann et al., unpublished data, 1994] for reconstructing the history of freshwater runoff from the northwest Sahara.

Methods and Strategy

The basic relationship between water temperature (T) and the $\delta^{18}O$ signal of carbonate is summarized in equation (1) [*O'Neil et al.*, 1969; *Shackleton*, 1974; *Duplessy et al.*, 1991]:

$$T = 16.9 - 4.38\left(\delta^{18}O_{carbonate} - \delta^{18}O_{water}\right) + 0.1\left(\delta^{18}O_{carbonate} - \delta^{18}O_{water}\right)^2 \quad (1)$$

This relationship is derived from a laboratory calibration of the isotope fractionation factor and is used as proxy for interpreting the $\delta^{18}O$ records of past temperature regimes. If paleo-

temperatures are known, (1) can be resolved to decipher the $\delta^{18}O$ composition of paleo water masses in which the carbonate precipitation has occurred, which mainly corresponds to the paleo salinity of a water mass, in addition to the global $\delta^{18}O$ ice effect. To estimate past SSS variations of the low-latitude Atlantic, the $\delta^{18}O$ signals of the surface dwelling species *G. ruber* (white) are used together with paleo SST data derived from counts of the faunal composition of planktonic foraminifera (SIMMAX transfer function, Pflaumann et al., submitted manuscript).

Both the isotopic composition and the salinity of sea surface water are influenced by the local evaporation/precipitation pattern, by lateral freshwater input, and by the global ice-volume effect during the glacial-interglacial cycles [*Duplessy*, 1978; *Labeyrie et al.*, 1987]. Accordingly, paleo SSS can be calculated from paleo SST and planktonic $\delta^{18}O$ values, using a $\delta^{18}O$-versus-salinity relationship of sea surface water to be defined in this paper, as shown in (2):

$$\text{Salinity} = f\left(\delta^{18}O_{G.ruber},\ \delta^{18}O_{ice},\ \text{paleo SST}\right) \qquad (2)$$

To arrive at a transfer function for paleo salinity values as outlined in (2), various calculation steps are necessary as summarized in Figure 1.

Note that because of a poorer correlation between calculated and measured SSS than between calculated and measured SST (see below), which originates from both the local frontal systems of SSS and the small SSS range covered by our data set, we tested the validity of our equations in the SST domain, where the range is much broader and hence the result more promising.

Development of a Transfer Function for SSS

Calibration of the Relationship Between Salinity and $\delta^{18}O$ Values of Sea Surface Water

Although SSS is linearly correlated with the $\delta^{18}O$ composition of sea surface water [*Geochemical Ocean Sections Study (GEOSECS) Excutive Committee*, 1987; *Duplessy et al.*, 1991], this relationship varies in different regions of the ocean [*Craig and Gordon*, 1965; *Ganssen*, 1983], because both salinity and $\delta^{18}O$ also depend on the origin of a particular surface water mass and the different sources of freshwater. For estimating paleo SSS in the low-latitude Atlantic, the regional $\delta^{18}O$-versus-salinity relationship has been derived from the GEOSECS data set collected in the Atlantic from 40°S to 40°N [*GEOSECS Excutive Committee*, 1987] using the best fit of least squares regression (equations (3) and (4)). Note that the $\delta^{18}O$-versus-salinity relationship is fairly constant in the surface water from different parts of the Atlantic (Figure 2). Hence we may assume that it won't have changed significantly in the past. If paleo salinity is deduced from a known isotopic composition of sea water (as independent variable), (3) is obtained (line A in Figure 2):

$$\text{Salinity} = 34.027 + 2.334\delta^{18}O_{water} \quad \text{(in SMOW)}$$

or

$$\text{Salinity} = 34.657 + 2.334\delta^{18}O_{water} \quad \text{(in PDB)} \qquad (3)$$

(In this equation the GEOSECS $\delta^{18}O_{water}$ data is adjusted by -0.27 from Standard mean ocean water (SMOW) to Pee Dee belemnite (PDB).)

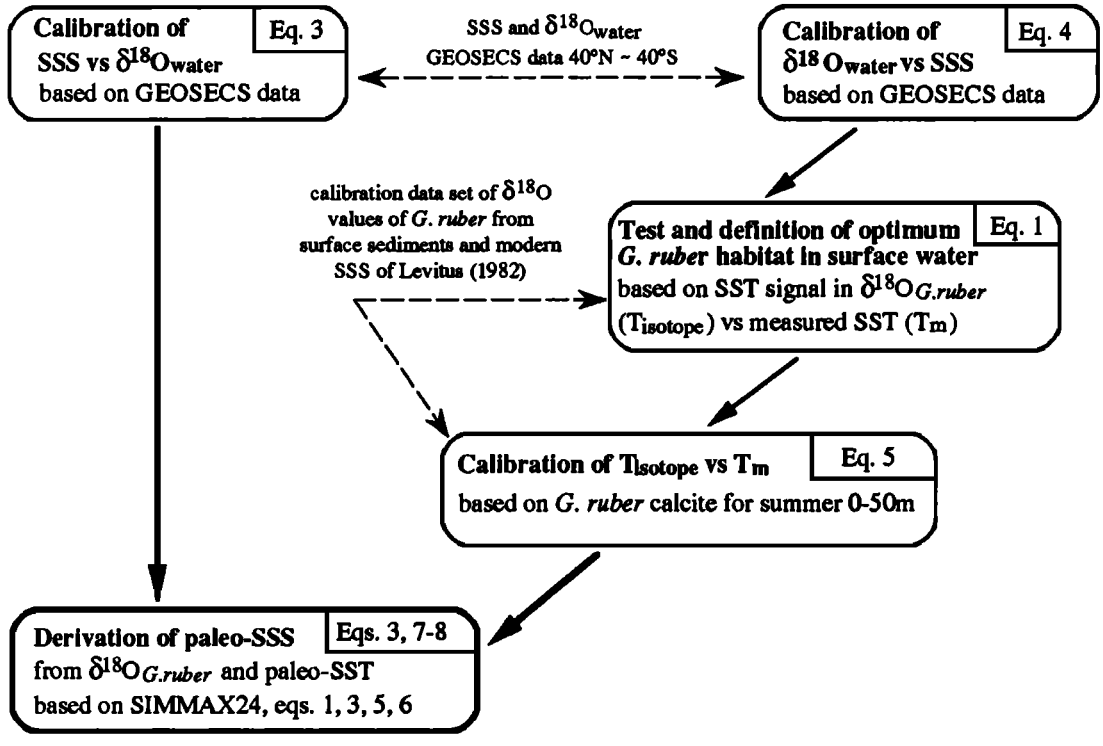

Figure 1. Strategy steps in developing transfer equation (8) for paleo SSS based on $\delta^{18}O$ values of *Globigerinoides ruber* (white) and paleotemperatures.

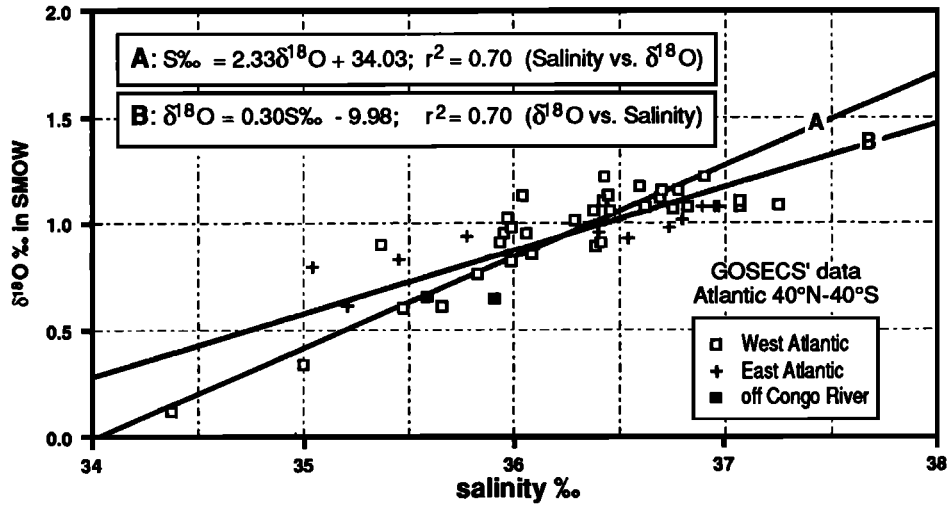

Figure 2. The $\delta^{18}O$ and salinity values of sea surface water (0-250 m) in the low-latitude Atlantic (40°N-40°S) [*GEOSECS Excutive Committee*, 1987]. Line A reflects regression of salinity versus $\delta^{18}O$ ratio; line B reflects regression of $\delta^{18}O$ versus salinity ratio.

On the other hand, if the isotope values are calculated from a known salinity (as independent variable), regression equation (4) is received (line B in Figure 2):

$$\delta^{18}O_{water} = -9.986 + 0.30\text{Salinity} \quad \text{(in SMOW)}$$

or

$$\delta^{18}O_{water} = -10.146 + 0.30\text{Salinity} \quad \text{(in PDB)} \quad (4)$$

Equations (3) and (4), the results of which appear different, are based on the same 46 pairs of measured salinity and $\delta^{18}O$ values. The correlation of the two variables is highly significant in each equation as shown by correlation coefficient of 0.84 (r^2 = 0.70; standard errors of 0.35‰ in salinity and 0.13‰ in $\delta^{18}O$, respectively).

Test of the Temperature-versus-$\delta^{18}O_{G.\ ruber}$ Relationship

Both the seasonal and depth distributions of a species contribute to the $\delta^{18}O$ composition of planktonic foraminiferal tests in the sediment [*Williams et al.*, 1981, *Hemleben et al.*, 1989]. Because the narrowly confined habitat of *G. ruber* mainly depends on temperature [*Tolderlund and Bé*, 1971; *Bijma et al.*, 1990; *Molfino*, 1993], the $\delta^{18}O$ signal of *G. ruber* tests reflects the water property for a small depth range of about 10-25 m in the surface ocean. Moreover, the $\delta^{18}O$ signal represents a certain season of the year, where and when most tests of *G. ruber* in a sediment assemblage have been produced, i.e., when the optimum temperature conditions for this species have prevailed [*Ganssen*, 1983; *Deuser*, 1987]. The $\delta^{18}O$ composition of *G. ruber* tests is in equilibrium with the ambient sea water, and thus the $\delta^{18}O$ values of sea water derived from (1) are subject to a habitat effect; more specifically, they depend on the temperatures occurring at particular water depths and certain seasons.

In order to apply the SST equation (1) to any $\delta^{18}O$ record of *G. ruber*, a proper calibration of the outlined habitat effect is necessary first to determine precisely which water layer and which season are reflected by the $\delta^{18}O_{G.ruber}$ signal. Subsequently, the relationship between (1) the modern SST and the subsurface temperature averages reflecting the optimum habitat of *G. ruber* and (2) the corresponding $\delta^{18}O$ isotopic temperature (T_{iso}) of *G. ruber* test is defined. Finally, this regression is employed for calculating the paleo SSS of the ambient water mass and the pertinent season where *G. ruber* has produced its test in isotopic equilibrium with sea water. T_{iso} was also reported as "effective temperature" by *Duplessy et al.* [1991].

The data set used for our calibration is composed of $\delta^{18}O$ values of *G. ruber* from 50 surface sediment samples in the low-latitude Atlantic (Table 1, Figure 3) and is based on published and unpublished data from Kiel University and other sources (Table 1). The 50 values of $\delta^{18}O_{G.ruber}$ were selected from altogether 170 core top data in the low-latitude Atlantic mostly recovered from the west African continental margin, because they probably represent the best approximation to the "genuine surface sediment" record. The selection was based on two criteria: (1) most of the samples were carefully picked from the top 1-3 cm core depth, and (2) the sedimentation rates at the core sites were equal to and/or higher than 2.5 cm/kyr based on accelerator mass spectrometry (AMS) ^{14}C analogue stratigraphy [*Winn et al.*, 1991] and direct dating (Table 1). At the samples from the eastern Gulf of Guinea, sedimentation rates are assumed to be high per analogy with dated local cores [Univ. of Kiel, unpublished data, 1993] and because of the strong local river discharge. Samples from very steep continental slopes (>5°) were discarded because of significant downslope sediment reworking in the nepheloid layer.

In summary, the 50 samples of our study may represent a sediment record of the last 400 to 1200 years and accordingly, the SSS and SST values reconstructed by $\delta^{18}O$ values of *G. ruber* may qualify for a calibration with modern SST and SSS data that probably represent an average of the last hundred years [e.g., *Levitus*, 1982]. We prefer $\delta^{18}O$ values measured on *G. ruber* from surface sediments to $\delta^{18}O$ values of specimens from plankton hauls and the Levitus SSS and SST data to in situ measurements because (1) the sediment data present a long-term average of the surface water hydrography; (2) the effects of calcium carbonate dissolution may be similar to the

Table 1. Oxygen Isotope and Hydrographic Data at the Core Top Sites in the Low-Latitude Atlantic Used for Developing a Transfer Equation for Paleo Salinity

Site	Latitude, °N	Longitude, °E	Water Depth, m	Corer Type,	Interval, cm	$\delta^{18}O$ *G.ruber* (White), ‰	Measured Temperature, T_m °C				Measured Salinity, S_m ‰				Isotopic Temperature, T_{iso} °C				Sedimentation Rate, cm/ky	Notes on Stratigraphy,	References
							summer		annual mean		summer		annual mean		summer		annual mean				
							0 m	0-50 m	0 m	0-50 m	0 m	0-50 m	0 m	0-50 m	0 m	0-50 m	0 m	0-50 m			
226	17.95	-21.05	3100	5	1	-1.11	25.17	22.60	22.89	21.31	35.99	36.04	36.05	36.12	24.69	24.76	24.77	24.87	25.00	AMS-analog	5
1113 -4	-5.75	-11.04	2374	1	1	-1.59	27.53	25.11	25.70	24.39	35.80	35.89	35.75	35.87	26.71	26.83	26.63	26.81	2.76	AMS-analog	4, 5
A172-6	14.98	-68.85	4160	6	20	-1.81	28.09	27.73	26.78	27.00	35.89	35.68	35.87	35.77	27.90	27.59	27.86	27.72	3.37	O18 stratigraphy	13
CH0182-36	26.18	-77.65	651	5	1	-1.74	28.38	27.99	26.30	25.94	36.44	36.48	36.38	36.41	28.36	28.41	28.27	28.31	3.61	C14-sediment	8
CH88-11P	30.67	-74.42	3337	6	4	-1.59	26.82	25.96	24.34	23.75	36.62	36.57	36.55	36.52	27.89	27.82	27.78	27.74	2.85	AMS 14C comp.	11
EN32-PC4	26.94	-91.36	2260	6	1	-1.87	28.51	26.65	25.11	24.00	36.19	36.27	36.05	36.20	28.63	28.75	28.42	28.64	10.11	C14-PF	10
EN32-PC6	26.95	-91.35	2280	6	0	-1.65	28.51	26.64	25.11	24.00	36.18	36.27	36.05	36.20	27.54	27.67	27.35	27.57	45.27	C14-PF	10
KW31	3.52	5.57	1515	6	22.5	-2.19	26.54	23.20	27.58	23.48	32.42	34.08	32.10	33.93	24.76	27.12	24.30	26.91	69.60	C14-PF+BF*	5†
LYII-13A	35.97	-7.82	1201	6	7.5	-0.23	21.74	19.83	18.61	17.65	36.28	36.29	36.25	36.26	21.01	21.02	20.96	20.98	7.69	AMS-analog	5
M12309 -1	26.84	-15.12	2849	3	0-1	-0.52	21.74	20.96	19.99	19.49	36.68	36.66	36.63	36.62	22.89	22.86	22.82	22.81	5.65	AMS-analog	2, 5
M12310 -3	23.50	-18.72	3076	1	1	-0.87	22.24	21.45	20.75	20.25	36.57	36.56	36.57	36.56	24.38	24.35	24.37	24.35	5.82	AMS-analog	4, 5, 12
M12327 -2	23.13	-17.41	1024	3	0-1	-0.80	21.27	20.47	19.59	19.12	36.46	36.45	36.46	36.43	23.89	23.87	23.88	23.85	5.97	AMS-analog	2, 5
M12328 -4	21.15	-18.57	2798	1	0-1	-1.42	22.80	21.23	20.76	19.79	36.27	36.27	36.26	36.27	26.56	26.56	26.55	26.56	12.00	AMS-analog	3, 5
M12329 -2	19.37	-19.93	3314	3	0-1	-1.23	24.41	22.08	22.07	20.63	36.08	36.11	36.10	36.15	25.39	25.42	25.41	25.48	2.90	AMS-analog	1, 4, 5
M12337 -4	15.95	-18.13	3094	1	0.75	-1.35	27.51	22.98	23.47	20.52	35.69	35.67	35.76	35.72	25.40	25.37	25.49	25.45	6.00	AMS-analog	5
M12345 -5	15.48	-17.36	966	3	0-1	-1.91	28.40	23.46	23.64	20.50	35.66	35.62	35.73	35.67	28.05	27.99	28.15	28.07	19.00	AMS-analog+14C	2, 5
M12347 -1	15.83	-17.85	2710	3	0-1	-1.84	27.68	23.07	23.48	20.49	35.69	35.66	35.75	35.71	27.76	27.71	27.84	27.78	10.50	AMS-analog+14C	1, 5
M12379 -3	23.13	-17.75	2064	4	0-1	-0.54	21.66	20.82	20.10	19.55	36.50	36.48	36.49	36.46	22.73	22.70	22.72	22.68	6.60	AMS-analog	2, 5
M12392 -1	25.17	-16.85	2575	4	3.25	-0.78	21.53	20.93	20.14	19.75	36.67	36.64	36.66	36.62	24.09	24.04	24.07	24.02	4.21	AMS-analog	4, 5
M13289 -1	18.08	-18.01	2470	2	0-1	-1.19	25.69	22.16	22.24	19.96	35.84	35.82	35.87	35.85	24.86	24.82	24.89	24.87	3.40	AMS 14C	1, 5
M13291 -1	18.12	-18.08	2696	4	0-3	-1.50	25.66	22.15	22.24	19.97	35.84	35.82	35.87	35.86	26.33	26.30	26.37	26.35	3.50	AMS-analog+14C	2, 2
M15637 -1	27.01	-18.98	3849	5	0-0	-0.71	22.79	22.19	21.31	20.92	36.86	36.85	36.85	36.83	24.03	24.01	24.01	23.99	3.75	AMS-analog	3
M15663 -1	34.92	-6.85	485	3	0-1	-0.67	22.80	20.49	19.19	18.05	36.37	36.37	36.36	36.35	23.16	23.16	23.14	23.12	3.96	AMS-analog	1, 7
M15666 -9	34.96	-7.12	798	3	0-1	-0.55	22.74	20.46	19.18	18.06	36.36	36.37	36.35	36.34	22.59	22.59	22.57	22.56	3.95	AMS-analog+14C	1, 5
M15669 -2	34.89	-7.82	1997	3	0-1	-0.55	22.19	20.17	19.07	18.04	36.34	36.34	36.33	36.32	22.56	22.55	22.54	22.53	3.21	AMS-analog+14C	1, 5
M15670 -1	34.91	-7.58	1460	3	0-1	-0.54	22.27	20.21	19.10	18.05	36.34	36.34	36.33	36.32	22.51	22.51	22.50	22.49	4.30	AMS-analog+14C	1, 5
M16004 -1	29.98	-10.65	1512	6	0.5	-0.19	21.48	19.77	19.06	18.20	36.48	36.46	36.45	36.42	21.10	21.06	21.06	21.02	3.60	AMS-analog	3, 4, 5
M16006 -1	29.25	-11.50	796	5	0-0	-0.03	21.72	19.93	19.26	18.36	36.47	36.46	36.45	36.43	20.33	20.31	20.30	20.27	6.17	AMS-analog	3, 5

Table 1. (continued)

Site	Latitude, °N	Longitude, °E	Water Depth, m	Corer Type,	Interval, cm	$\delta^{18}O$ *G.ruber* (White), ‰	Measured Temperature, T_m °C				Measured Salinity, S_m ‰				Isotopic Temperature, T_{iso} °C				Sedimentation Rate, cm/ky	Notes on Stratigraphy,	References
							summer		annual mean		summer		annual mean		summer		annual mean				
							0 m	0-50 m	0 m	0-50 m	0 m	0-50 m	0 m	0-50 m	0 m	0-50 m	0 m	0-50 m			
M16030	-1 21.24	-18.06	1500	4	0.8	-1.15	22.41	20.76	20.19	19.18	36.22	36.20	36.21	36.19	25.20	25.18	25.19	25.17	6.12	AMS-analog	6, 5
M16402	-1 14.42	-20.57	4203	1	0-1	-1.00	26.97	22.60	24.47	21.48	35.70	35.72	35.81	35.79	23.77	23.79	23.92	23.88	3.20	AMS-analog	2, 5
M16457	-2 5.40	-21.72	3308	5	0-1	-1.66	27.90	26.79	27.49	25.79	35.22	35.58	35.26	35.52	26.21	26.73	26.27	26.64	4.53	AMS-analog	2, 5
M16772	-1 -1.34	-11.97	3991	1	0.75	-1.49	28.19	24.87	26.27	24.18	35.20	35.56	35.29	35.54	25.37	25.88	25.49	25.85	3.44	AMS-analog	5, 6
M16773	-1 -0.97	-9.44	4662	6	1	-1.31	27.91	24.26	25.93	23.56	34.96	35.41	35.12	35.44	24.18	24.82	24.40	24.86	2.55	AMS-analog	5, 7
M16854	-1 6.017	3.608	1583	1	0-1	-1.85	27.10	23.58	28.05	24.94	30.07	32.83	31.95	33.72	19.94	23.73	22.50	24.98	u	per analogy	17†
M16855	-1 5.51	3.78	2173	1	0	-2.32	27.10	23.55	28.00	24.80	30.08	32.85	32.39	33.98	22.10	25.98	25.33	27.60	u	per analogy	17†
M16862	-1 3.547	6.487	698	1	0-1	-2.27	26.40	22.75	27.55	23.95	31.80	33.88	32.60	34.15	24.26	27.21	25.39	27.61	u	per analogy	17†
M16864	-1 3.155	6.285	1495	1	0-1	-2.18	26.30	22.70	27.50	23.95	32.00	33.98	32.70	34.21	24.12	26.92	25.10	27.27	u	per analogy	17†
M16865	-1 2.67	6.06	2492	1	0	-1.94	26.25	22.68	27.48	24.01	34.08	34.99	33.64	34.68	25.92	27.23	25.30	26.78	u	per analogy	17†
M16866	-1 2.002	5.718	3501	1	0-1	-2.11	26.04	22.38	27.23	23.44	32.17	34.01	32.57	34.19	24.03	26.64	24.58	26.89	u	per analogy	17†
M16867	-1 -2.20	5.10	3891	1	1	-1.45	24.16	22.26	26.27	23.41	35.13	35.45	34.31	34.89	25.08	25.54	23.93	24.74	2.50	AMS-analog	5, 6†
M16869	-1 -0.21	6.01	1837	1	0-1	-1.71	25.02	21.58	26.72	23.16	32.70	34.31	33.39	34.62	22.90	25.16	23.86	25.59	u	per analogy	17†
M16870	-1 0.21	5.97	2469	1	0	-1.08	25.02	21.58	26.72	23.16	33.98	34.88	33.32	34.59	21.75	23.00	20.85	22.59	u	per analogy	17†
M16871	-1 -0.73	6.935	2987	1	0-1	-1.49	24.64	21.35	26.58	23.11	32.45	34.19	33.28	34.56	21.54	23.95	22.67	24.47	u	per analogy	17†
M16872	-1 -0.35	8.04	2987	1	0-1	-1.77	24.71	21.53	26.78	23.36	31.55	33.76	32.36	34.11	21.59	24.65	22.71	25.15	u	per analogy	17†
MG237	-5.20	11.33	1000	5	15	-2.18	29.12	23.33	25.77	22.42	30.48	33.12	31.98	33.86	22.01	25.69	24.09	26.75	20.50	C14	5
V22-174	-10.0	-12.8	3252	5	0	-1.23	26.57	25.34	25.31	25.02	36.43	36.43	36.22	36.37	25.88	25.88	25.58	25.80	2.63	AMS-analog	7, 9
V22-222	28.93	-43.65	3197	6	0	-0.87	26.44	25.14	23.56	22.87	36.87	36.87	36.90	36.91	24.80	24.80	24.84	24.85	2.73	C14 of $CaCO_3$	14
V26-176	36.05	-72.38	3942	5	0	-1.35	25.19	23.48	21.73	20.77	35.86	35.99	35.69	35.87	25.64	25.82	25.40	25.66	15.00	AMS C14-PF	11, 5
V30-49	18.43	-21.08	3093	5	5-7	-1.05	25.05	22.59	22.79	21.30	36.02	36.07	36.08	36.15	24.45	24.52	24.53	24.63	2.50	AMS-analog	2, 5, 7
V32-08	34.78	-32.42	3252	6	1	-0.56	24.47	22.40	20.94	19.84	36.32	36.31	36.39	36.37	22.58	22.56	22.68	22.65	3.23	C14 of $CaCO_3$	16

Core types are 1, Giant box core; 2, Box core; 3, Grab core; 4, Kasten core; 5, Gravity core; 6, Piston core. References are 1, *Ganssen*, 1983; 2, *Jung*,1990; 3, *Zahn-Knoll*, 1986; 4, *Winn et al.*, 1991; 5, M. Sarnthein, unpublished data, 1994; 6, K. Winn, unpublished data, 1994; 7, H. Schulz, unpublished data, 1994; 8, *Slowey and Curry*, 1987; 9, *Shackleton*, 1977; 10, *Flower and Kennett*, 1990; 11, *Keigwin and Jones*, 1989; 12, *Hommers*, 1979; 13, *Emiliani*, 1955; 14, *Mix et al.*, 1986; 15, *Imbrie and Kipp*, 1971; 16, *Mix and Ruddiman*, 1985; 17, This paper. Measured sea surface temperature and salinity are interpolated from *Levitus* [1982] and *Kolesnikov* [1973]. Sedimentation rate is calculated for Holocene only (u = unknown).

* PF, BF, mixed planktonic or benthic foraminifera sample.

† Northern hemisphere seasons are used at sites in Gulf of Guinea.

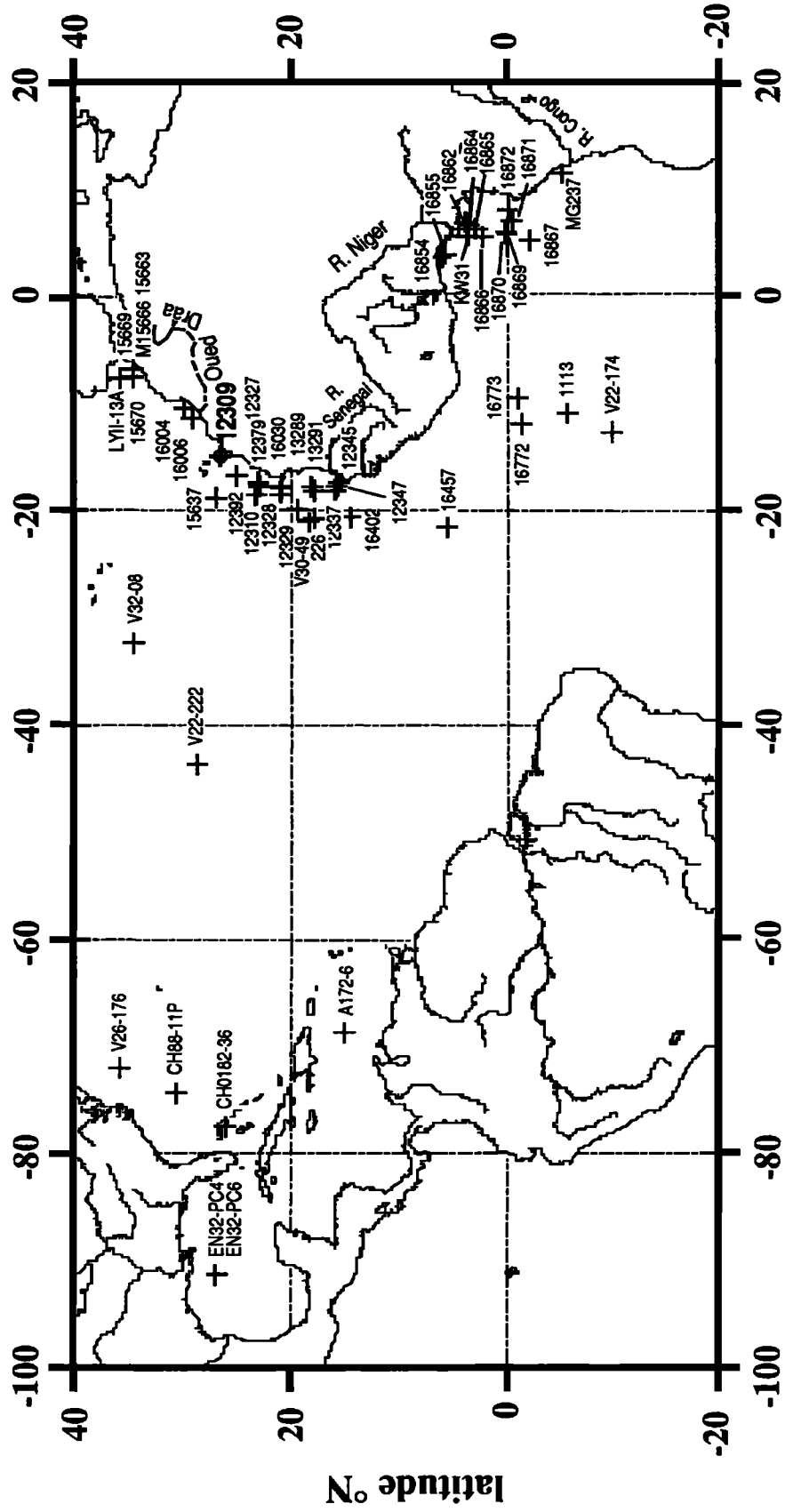

Figure 3. Site locations of core top samples with $\delta^{18}O$ values of *G. ruber* (white) used for testing the temperature-versus-$\delta^{18}O_{G.\ ruber}$ relationship. Core site 12309-2 is marked in bold.

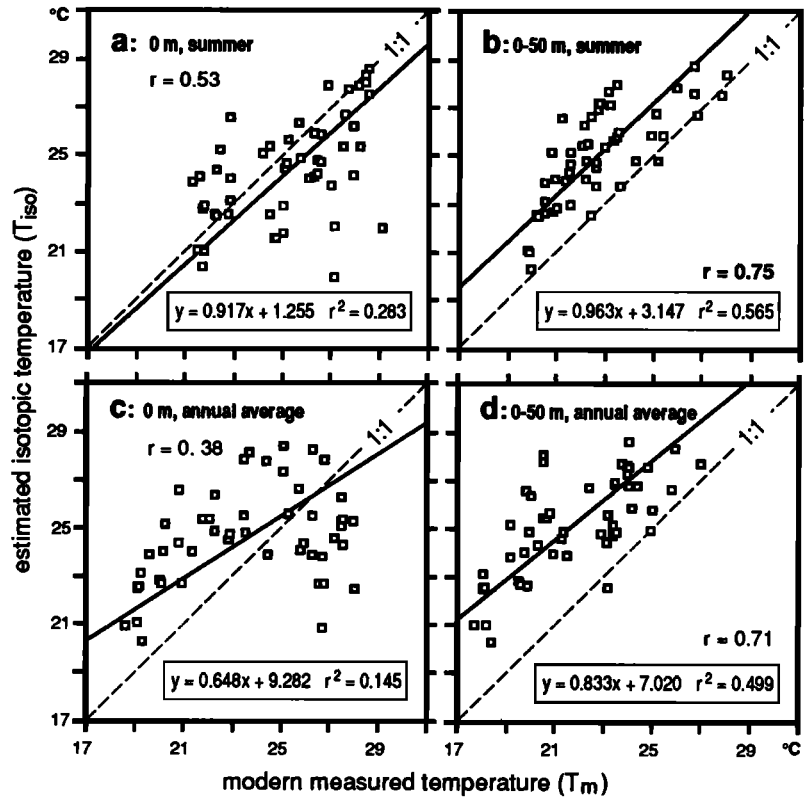

Figure 4. Comparison of measured SST [*Levitus*, 1982] (T_m) and isotopic SST (T_{iso}) calculated from $\delta^{18}O$ values of *G. ruber* and measured SSS [*Levitus*, 1982]. Four different cases help to determine the dominant habitat of this species, which controls $\delta^{18}O$ values/SSS signals of their carbonate tests: (a) summer SST at sea surface (0 m), (b) summer SST at 0-50 m water depth, (c) annual SST at sea surface (0 m), and (d) annual SST at 0-50 m water depth. Note the best correlation between T_m and T_{iso} in case of Figure 4b. Regression lines are based on "Reduced Major Axis" method of *Davis* [1986]

effects encountered at samples further downcore; and (3) the sediment record provides a data set comprising a broader SST/SSS range in the east Atlantic than any set of plankton haul data. However, at nearshore hydrographic frontal systems linked to fluvial freshwater input (e.g., off the Niger and Congo deltas), the Levitus data were replaced by regional synoptic data set such as the EQUALANT atlas [*Kolesnikov*, 1973]. These data clearly depict small-scale plumes of low-salinity surface water, which otherwise are smoothed largely away by the data treatment of *Levitus* [1982]

Isotopic SSTs (T_{iso}) are compared (Figure 4) with various sets of modern SST data (T_m) [*Levitus*, 1982; *Kolesnikov*, 1973]. T_{iso} values are calculated via (1) from $\delta^{18}O_{G.\ ruber}$ values and from measured SSS of the pertinent water horizon to deduce $\delta^{18}O_{water}$ via (4). In the regressions of Figure 4, the summer and annual Levitus SSS values of both the true surface (0 m) and the average at 0-50 m are employed alternatively (i. e., summer at 0 m, annual average at 0 m, summer at 0-50 m, and annual average at 0-50 m). To achieve a match between the data obtained from the two hemispheres, the Levitus data from opposite caloric seasons are combined. That means February to April (i.e., summer) data from the south are lumped with August to October data from the north. In the Gulf of Guinea, however, data of the northern summer must be employed, because here the regional river discharge is clearly linked to precipitation maxima during northern summer (drainage basins at 5-15°N). This implies that summer SST values in the Gulf of Guinea are lower than the annual average values (Table 1)

The best correlation between T_{iso} and T_m exists in the case of summer temperatures at 0-50 m with a significant relationship of $r = 0.75$. This demonstrates that in the low-latitude Atlantic, or more accurately, in the region represented by the calibration data set, $\delta^{18}O$ values of *G. ruber* tests mainly reflect the summer temperature and salinity of the topmost 50 m in the surface ocean (Figure 4), although, to some degree, the tests are a product of all seasons.

In Figure 4b, the slope of the regression line of 0.963 comes close to a 1:1 correlation, if we use the Reduced Major Axis approach (RMA) described by *Davis* [1986] instead of the least squares regression technique. The RMA procedure minimizes the product of the deviations in both the X and the Y directions of a wide scattered bivariate data matrix. It is useful in expressing the mutual relationship between two variables which are both subject to errors and neither can be regarded as a function of the other such as in our case. The RMA is defined by an ordinary linear equation. The slope is defined as the ratio of the standard deviations of the two variables and in our case those of the T_{iso} and T_m. The RMA of Figure 4b results in (5),

$$T_{iso} = 3.147 + 0.963 T_m \quad (5)$$

Based on SSTs calculated from (5), paleo SSS at 0-50 m can now be deduced from (2) for the summer season.

The standard error of (5) is ±1.43°C. The systematic deviation of the regression line from the 1:1 correlation is about 2.5°C in the temperature range 18-28°C. The shift originates from both the preferential near-surface habitat and the short-term seasonal timing of *G. ruber*. Finally, this deviation has to be considered for the paleo salinity calculation via the correction of all paleo SST estimates according to (5). On the basis of various long $\delta^{18}O$ records of *G. ruber* (mainly unpublished University of Kiel records) comprising the last 2-3 glacial cycles, we assume that this $\delta^{18}O$ versus SST relationship has remained constant over the last 250 to 350 kyr, because the $\delta^{18}O$ level of glacial and interglacial oscillations remained unchanged.

The Transfer Equation for Paleo-Salinity

Using the $\delta^{18}O$ value of *G. ruber* tests and measured and/or reconstructed summer temperatures for 0-50 m (T_m) which are characteristic of the habitat of this species, the $\delta^{18}O$ value of sea water ($\delta^{18}O_{water}$) can be calculated from (1) if T is replaced by T_m (using (5)) as shown in (6) to take into account of the habitat effect of *G. ruber*:

$$\delta^{18}O_{water} = \delta^{18}O_{G.\,ruber} - 21.9 + \sqrt{310.6 + 10\left(0.963 T_m + 3.147\right)} \quad (6)$$

Finally, SSS can be estimated by inserting (6) into (3) as shown in (7). This approach is based on the assumption that the relationship between the salinity and $\delta^{18}O_{water}$ of the present sea surface water masses does not change through past times in the low-latitude Atlantic, because there is no significant spatial variation in the modern data (Figure 2):

$$SSS = 34.657 + 2.334\left(\delta^{18}O_{G.\,ruber} - 21.9\right) + 2.334\sqrt{310.6 + 10\left(0.963 T_m + 3.153\right)} \quad (7)$$

The standard error of the salinity estimates from (7) can be assessed on two ways. First, the error can be calculated directly by adding the errors of the two transfer equations contained in (7), which amount to ±0.35‰ SSS for (3) and ±0.69‰ SSS (corresponding to ±1.43°C) for (5), leading to an additive standard error of ±0.77‰ SSS [Hartung, 1989]. Further analytical uncertainties in paleo SST estimates and oxygen isotope measurements (< ±1°C equal to about 0.5‰ SSS and < ±0.1‰ $\delta^{18}O$, respectively) sum up to an additive error of about 0.6‰ SSS, which is about equal to the standard error in (7) itself.

On the other hand, the standard error can be derived from a direct comparison of modern measured versus calculated salinity values (Table 1 and Figure 5). The standard error of this regression is ±0.72‰ for salinity, which is a range similar to the error found by the first approach. If (7) is employed for reconstructing paleo salinities, one has to take into account regional small-scale SSS gradients of 2-4‰ in the modern low-latitude Atlantic and glacial-to-interglacial salinity changes amounting to about 1.0-1.5‰ because of the global ice effect. In this case, (7), with its standard error of ±0.72-±0.76‰, is promising to reveal, at least, the general trend of salinity fluctuations, especially along the ocean margins where the continental freshwater input may have changed significantly along with changes in low-latitude climate.

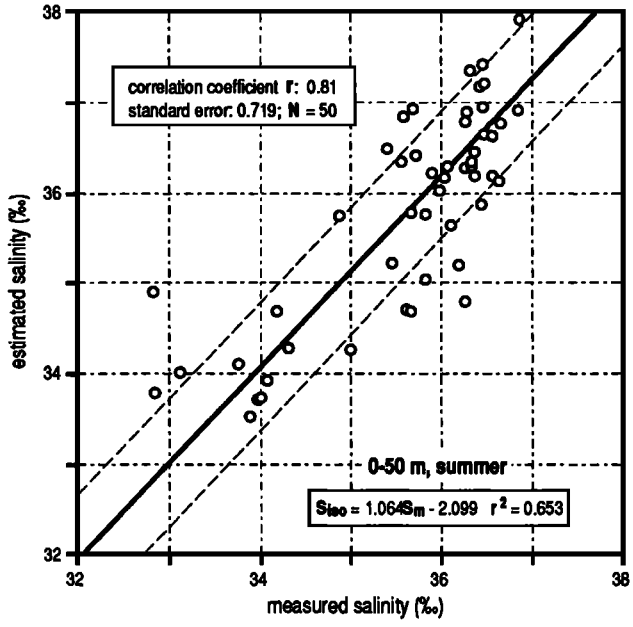

Figure 5. Comparison of measured summer salinity (0-50 m water depth) [*Levitus*, 1982] and isotopic salinity estimates calculated from $\delta^{18}O$ values of *G. ruber* (equation 8) and summer SST (0-50 m water depth) [*Levitus*, 1982, *Kolesnikov*, 1973] Differences between the paleo SSS estimates using equation of this paper (8) and equation (9) of *Rosteck et al.* [1993]

The Role of the $\delta^{18}O$ Ice Effect

Past changes in global ice volume during glacial-to-interglacial cycles imply that both $\delta^{18}O_{water}$ and SSS values calculated by means of (6) and (7) have been enlarged by the global ice effect during glacial times by an amount yet to be defined precisely. Local SSS variations that record changes of the regional climate are only linked to changes in the local freshwater input and evaporation/precipitation regime. Hence these figures can be estimated more precisely by subtracting the effects of sea level changes on global salinity and $\delta^{18}O_{water}$ changes from our overall salinity estimates based on (6) and (7). We are using the estimates of the global $\delta^{18}O$ ice effect derived from the U/Th dated sea level curve, which amount to 1.3‰ for the last glacial-to-interglacial transition [*Fairbanks and Matthews*, 1978; *Fairbanks*, 1989, 1990; *Bard et al.*, 1990]. Beyond 30.47 calendar (cal) kyr B.P., we employ the ice effect curve published by *Labeyrie et al.* [1987] and *Vogelsang* [1990], as summarized in (8).

$$SSS_{local} = 34.657 + 2.334\left(\delta^{18}O_{G.\,ruber} - \delta^{18}O_{ice} - 21.9\right) + 2.334\sqrt{310.6 + 10\left(0.963 T_m + 3.147\right)} \quad (8)$$

This transfer equation assumes that the modern ratio of 1‰ change in $\delta^{18}O_{water}$ equating to 2.334‰ SSS (equation 3) has been constant through all times. On the basis of this assumption, (8) can serve for estimating past changes in local summer salinity within the top 50 m of surface water in the low-latitude Atlantic.

Test Records: East Atlantic Paleo Salinity Variations off the Northwest Sahara

The $\delta^{18}O$ curves of *G. ruber* and paleotemperature records of Meteor core 12309-2 (26°50.3'N, 15°06.6'W, 2820 m water depth) serve as an example to estimate the local variations in paleo SSS based on the outlined reconstruction strategy. These data (Table 2) promise important insights into the changes of the freshwater input along the east Atlantic continental margin and hence of the rates of North African precipitation and evaporation. Modern salinity at site 12309-2 is purely controlled by the salinity of both the Canary Current and upwelled North Atlantic Central Water (NACW) during summer [*Sarnthein et al.*, 1982b], the salinity of which is fairly high (≥ 37.25‰ in both the source region of downwelling and at about 200 m depth; [*Levitus*, 1982; *Bainbridge*, 1981]). Today, no freshwater input from the North Sahara is recognized south of the rare floods of the Wadi Drâa mouthing near 28°40'N (Figure 3).

In Figure 6a, we compare a $\delta^{18}O$ curve of *Cibicidoides wuellerstorfi*, used for stratigraphic classification (see age marks in cal year), with the $\delta^{18}O$ signal of *G. ruber* serving as base for our paleo salinity reconstruction. On the basis of *Winn et al.* [1991], the sedimentation rates in core 12309-2 range from 5.6 cm/kyr in the Holocene to 11.5 cm/kyr in glacial times. Hence our 5-cm average sampling space enables us to resolve time spans of 900 years in the Holocene and 450 years in the glacial and across Termination I. The variations in the global $\delta^{18}O$ ice effect ($\delta^{18}O_{ice}$ in equation (8)) are defined by the U/Th dated sea level curve between 0 to 30.47cal ka B.P. [*Fairbanks*, 1990; *Bard et al.*, 1990] and between 30.15 to 40 cal kyr B.P. by the $\delta^{18}O_{ice}$ curve of *Labeyrie et al.* [1987] and *Vogelsang* [1990], the data of which have been found to be less reliable in our test calculation. The composite $\delta^{18}O$ curve is adjusted to a LGM-versus-interglacial $\Delta\delta^{18}O$ ice value of 1.3‰ [*Fairbanks*, 1989].

As shown in Figure 6b, the relative abundance of *G. ruber* (white) varies from a few tenths of a percent during glacial times to nearly 10% in the mid Holocene. Hence the oxygen isotope signals of *G. ruber* are strongly affected by downcore bioturbation of *G. ruber* tests across glacial Termination I as compared to the much less distorted benthic $\delta^{18}O$ record of *C. wuellerstorfi* that has occurred more persistently over glacial-to-interglacial times [*Lutze et al.*, 1979]. To account for this bioturbational shift of the $\delta^{18}O_{G.ruber}$ signal, the $\delta^{18}O$ curves of *G. ruber* were adjusted to the $\delta^{18}O$ stratigraphic record of *C. wuellerstorfi* using three age control points that can be recognized easily in most $\delta^{18}O$ records, that is, the end (17.1 cal kyr) and the beginning (18.3 cal kyr) of Termination IA and oxygen isotope event 3.1 (29.5 cal ka; arrows in Figure 6a). The ages between the three switch points were adjusted by telescoping based on the assumption of constant sedimentation rates in between.

In the top 50 m water depth, summer temperatures varied moderately by 3 °C over the last 38,000 years (Figure 6c, Table 2). A unique abrupt warming by 3 °C occurred at the end of the LGM (after 18,000 yr B.P.). The small-scale short-term SST variability at 27-19 cal kyr B.P. (Δ1.8°C) is little substantiated by data. In summary, one may expect that past SST variations have generally influenced the reconstructed variations in paleo SSS by less than 0.5-0.75 ‰, except for the SST rise during early Termination I which corresponds to about Δ1.5‰ SSS.

The variations in summer SSS (Figure 6d, Table 2) based on (8) suggest significant and reasonable changes in hydrography over the last glacial cycle. During the last glacial, local salinity generally exceeded the Holocene level by about 0.5-1.0‰ reaching 37.2-38.1‰, in addition to changes linked to the variations in global ice volume. Likewise, summer SSS was high during late stage 3, although this stage is poorly resolved. An extreme maximum (38.2‰) occurred right after Termination IA [*Duplessy et al.*, 1981] near 14.5 cal kyr B.P (equal to 12.5 k ^{14}C yr B.P.).

Table 2. Oxygen Isotope Values, Paleo SST Values Estimated by SIMMAX24, and Paleo SSS Estimated by equation (8) of Core M12309

No. of sample M12309	Age in Calendar Years, × 1000	$\delta^{18}O$ *G. ruber* (white), ‰ PDB	Paleo SST Estimates (interpolated), °C	$\delta^{18}O$ ice effect (interpolated), ‰ PDB	Paleo SSS Estimates for 0-50 m, ‰
1	0.00	-0.52	20.20	0.00	36.40
2	0.22	-0.32	20.20	0.00	36.86
3	1.11	-0.39	20.39	0.00	36.79
4	1.99	-0.31	20.30	0.00	36.93
5	2.87	-0.45	20.73	-0.01	36.83
6	3.76	-0.35	20.67	-0.02	37.08
7	4.64	-0.35	20.82	-0.04	37.19
8	5.53	-0.64	20.82	-0.04	36.51
9	6.47	-0.62	20.26	0.05	36.08
10	7.58	-0.61	20.24	0.11	35.96
11	8.69	-0.45	20.00	0.12	36.18
12	9.80	-0.01	20.43	0.21	37.20
13	10.24	-0.33	20.24	0.22	36.34
14	10.68	-0.01	19.97	0.23	36.94
15	11.13	0.24	19.75	0.24	37.40
16	11.57	0.17	19.89	0.25	37.28
17	11.97	0.51	19.62	0.25	37.93
18	12.26	0.67	19.47	0.26	38.22
19	12.55	0.62	19.50	0.26	38.10
20	12.85	0.49	19.64	0.27	37.86
21	13.14	0.57	19.63	0.28	38.00
22	13.43	0.69	19.53	0.31	38.16
23	14.01	0.52	20.66	0.37	38.18
24	14.59	1.08	20.90	0.43	39.46
25	17.50	0.73	18.70	0.59	37.20
26	18.00	1.29	18.38	0.77	37.92
27	18.50	1.62	18.12	0.96	38.13
28	19.49	1.44	18.32	1.05	37.60
29	20.48	1.21	19.69	1.01	37.83
30	20.58	1.11	19.86	1.00	37.69
31	21.47	1.29	18.60	0.94	37.64
32	22.56	1.51	19.35	0.95	38.49
33	23.45	1.62	19.61	1.01	38.76
34	24.19	1.47	19.01	1.00	38.12
35	24.54	1.22	18.64	1.00	37.37
36	25.18	1.28	18.97	0.97	37.74
37	26.17	1.37	19.63	0.85	38.55
38	26.52	1.51	19.88	0.80	39.12
39	27.16	1.41	18.93	0.73	38.57
40	28.50	1.12	19.55	0.51	38.72
41	32.04	0.99	19.65	0.63	38.19
42	35.58	1.21	20.29	0.63	39.00
43	37.35	1.08	19.93	0.64	38.51

SIMMAX24 is the transfer function for estimating paleo SST from planktonic foraminifera assemblage (Pflaumann et al. submitted manuscript).

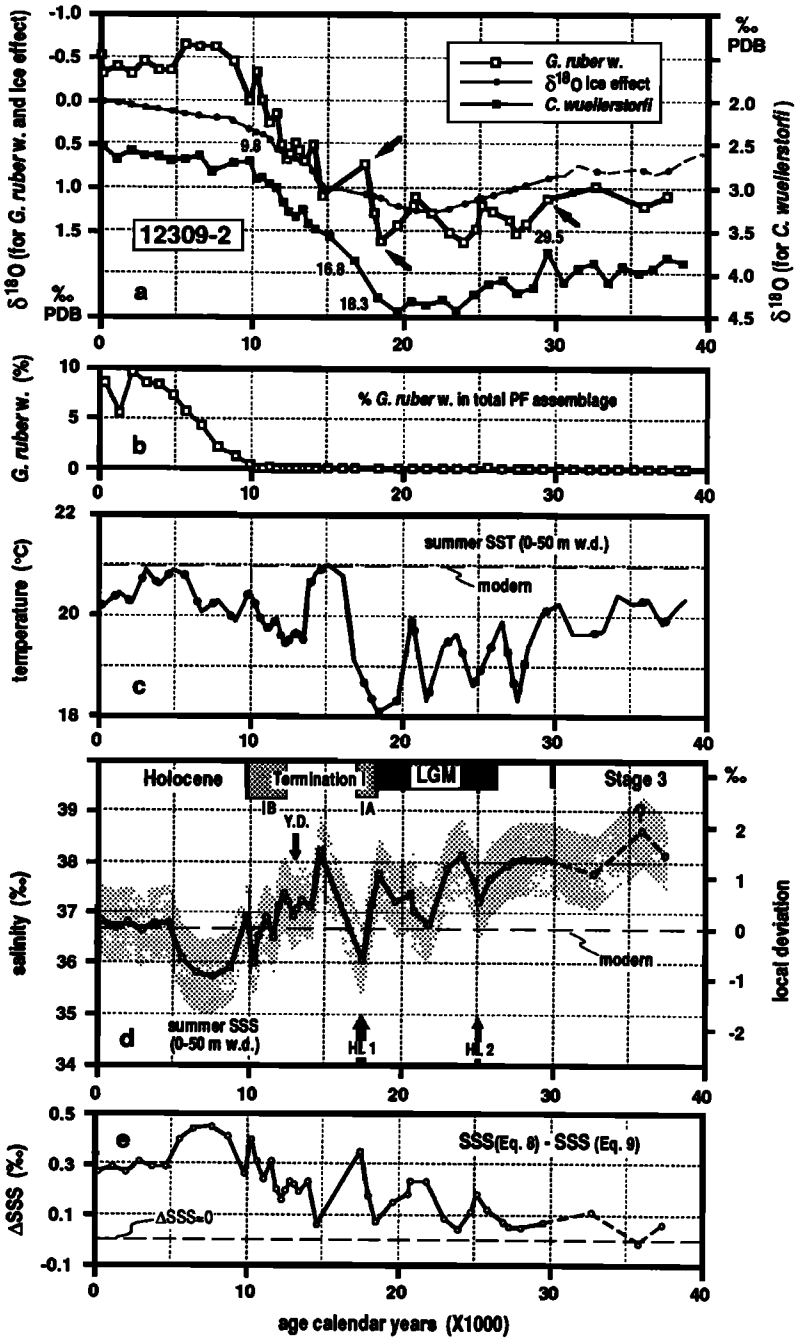

Figure 6. Reconstruction of local paleo salinity changes at the east Atlantic margin, about 27°N, over the last 37,000 years, based on proxydata of Meteor core 12309-2. (a) Oxygen isotope values of *G. ruber* (white) compared with $\delta^{18}O$ record of *C. wuellerstorfi* (315-400 μm) [*Zahn-Knoll*, 1986] used for age control [*Winn et al.*, 1991; *Alley et al.*, 1993; M. Sarnthein, unpublished data, 1993]. Numbers indicate calendar year B.P. (×1000). Global $\delta^{18}O_{ice}$ record is after U/Th dated sea level curve of the last 30.47 kyrs [*Fairbanks*, 1989, 1990; *Bard et al.*, 1990; *Fairbanks and Matthews*, 1978] and after global $\delta^{18}O$ ice effect curve of *Labeyrie et al.* [1987] and *Vogelsang* [1990] between 31.5 to 40.0 cal kyr B.P. Conventional ^{14}C ages are converted to calendar years following the technique of *Winn et al.* [1991]. Solid circles on $\delta^{18}O$ ice effect curve match the $\delta^{18}O_{G.\ ruber}$ data. Arrows mark major age control points, where the *G. ruber* record is adjusted to the $\delta^{18}O$ record of *C. wuellerstorfi*. (b) Percentage of *G. ruber* (white) in total planktonic foraminiferal assemblage >149 μm. (c) Summer sea surface temperatures (SST) curve for 0-50 m depth based on SIMMAX24 transfer function of Pflaumann et al. (submitted manuscript) and faunal counts of *Thiede* [1977]. Solid circles on this curve indicate interpolated SST estimates matching in age the level of $\delta^{18}O_{G.\ ruber}$ data. (d) Paleo SSS curve and standard errors (shaded area) estimated using equation (8). (e) Differences between the paleo SSS estimates using equation of this paper (8) and equation (9) of *Rosteck et al.* [1993]

Four factors may induce such changes in local SSS along the east Atlantic margin, near site 12309-2: (1) a decrease or increase in the continental runoff from the nearby northern Sahara; (2) changes in both the coastal upwelling intensity of the highly saline NACW and its original salinity values, for example, by variations in the precipitation-evaporation ratio over the subtropical North Atlantic; (3) changes in the dynamics of the Canary Current and its salinity; and (4) local changes in the precipitation-evaporation ratio at core site 12309.

As the modern continental runoff near site 12309-2 is already zero, the clearly increased salinity during the last glacial maximum (LGM) and stage 3 (36.9-38.1‰) and especially the SSS maximum after Termination IA (38.2‰) may be best explained by a differential advection of the less saline Canary Current water (<36.5‰; *Levitus* [1982]) and/or by culminations in the upwelling of NACW, the salinity of which (>37.2‰; *Bainbridge* [1981]) may have increased significantly. Local evaporation is probably less important because the salinity at site 12309 appears largely controlled by the high current dynamics in this region. These conclusions are corroborated by the glacial SSS range found in the subtropical North Atlantic, which has reached a level of 37.25-37.75‰ [*Duplessy et al.*, 1991], which is almost as high as the peak values in core 12309. Moreover, increased zonal SST anomalies (east Atlantic margin versus central Atlantic) demonstrate that the glacial intensity of coastal upwelling was much enhanced [*Pflaumann*, 1980; *Climate: Lang-Range Interpretation, Mapping, and Prediction* (CLIMAP) *Project Members*, 1981; *Sarnthein*, 1982] and thus the advection of NACW. We surmise that either a short-term culmination in the upwelling of highly saline NACW and/or a turnoff of the advection of cold and less saline Canary Current water from the north may best explain the special short lasting salinity spike (Δ2‰) near 14.5 cal kyr B.P. Note that it is coeval with the sudden postglacial restoration of the Atlantic Salinity Conveyor Belt, subsequent to the great meltwater event of the Heinrich layer 1 [*Sarnthein et al.*, 1994]. A well defined extreme SST maximum provides evidence for either processes (Figure 6c) by forming the base of maximum evaporation in the northeast Atlantic. A medium high salinity of 37.0-37.4‰ persisted until the Younger Dryas (about 12.0 cal kyr B.P.).

The glacial high salinities offshore northwest Africa confirm the complete lack of freshwater discharge from the North Sahara during the LGM and major parts of Termination I, which has been also suggested by numerous evidence from continental, lacustrine, and marine sediment records [*Sarnthein*, 1978, *Rossignol-Strick and Duzer*, 1979; *Koopmann*, 1981; *Sarnthein et al.*, 1982a, b; Street-Perrott et al., 1989;] and, moreover, by recent climate models [*Prentice*, 1992].

On the other hand, the various salinity lows during the last 40 kyr may record (1) increased continental runoff, (2) a breakdown in the upwelling of NACW, and (3) a lateral advection of low-salinity sea water from the north via the Canary Current. Thus these minima are difficult to interpret. In the early Holocene from 9.0 to 5.5 ka, the salinity was extremely reduced, by up to 1‰ lower than today. These phases parallel a period of pronounced humidity and high lake levels in the northern and southern Sahara [*Sarnthein*, 1978; *Rossignol-Strick and Duzer*, 1979; *Street and Grove*, 1979; *Sarnthein et al.*, 1982a, b; *Hooghiemstra et al.*, 1987; *Ritchie and Haynes*, 1987; *Petit-Maire*, 1989]. Hence a major portion of this low-salinity signal can be attributed to the continental runoff through the Wadis of South Morocco, which has fed the Canary Current. The other part of the early Holocene salinity reduction may be related to a reduction in coastal upwelling of NACW, a feature clearly evidenced also by paleoecological evidence [*Petit-Maire*, 1980] and reduced zonal SST anomalies [*Pflaumann*, 1980] for the early-to-middle Holocene. At 10.0 cal kyr B.P., however, the upwelling was still stronger than today [*Schulz*, 1994].

The two salinity lows (Δ1.6‰) at about 17.5 and 24.5 cal kyr ago, which are coeval with the long-term LGM aridity maximum in the Sahara [*Sarnthein*, 1978; *Rossignol-Strick and Duzer*, 1979; *Street and Grove*, 1979; *Sarnthein et al.*, 1982b; *Hooghiemstra et al.*, 1987], can hardly be assigned to continental runoff. They rather indicate short lasting complete breakdowns of coastal upwelling and coincide precisely in age with the great North Atlantic meltwater events linked to Heinrich layers 1 and 2 [*Bond et al.*, 1992, 1993; *Sarnthein et al.*, 1992, and M. Sarnthein et al., Variations in surface ocean circulation in the northern North Atlantic over the last 55,000 years: A timeslice record, submitted to Paleoceanography, 1994; hereinafter referred to as Sarnthein et al., submitted manuscript]. Hence, these salinity lows probably also record, for the first time, a southward advection of meltwater via the Canary Current into subtropical latitudes, an advection that helped suppressing the upwelling activity. A similar explanation may apply to the extremely short lasting (~500 years) salinity low prior to 10 cal kyr B.P. Further high-resolution paleo salinity records may help to trace more precisely these meltwater signals down to low latitudes and to uncover their implications for African continental aridity and humidity [L. Wang et al., manuscript in preparation, 1995].

Finally, in Figure 6e we show SSS anomalies that result from the difference between the results produced by our equation (8) and those produced by equation (9) of *Rosteck et al.* [1993]:

$$SSS_{local} = S_m + \left(\Delta\delta^{18}O_{G.\,ruber} - b\Delta T - \delta^{18}O_{ice}\right)/c \qquad (9)$$

This equation (9) was recently developed for the equatorial Indian Ocean, where S_m is modern salinity (i.e., 36.68‰), $\Delta\delta^{18}O_{G.\,ruber}$ is the difference between $\delta^{18}O_{G.\,ruber}$ values of downcore samples and the core top value (-0.52‰), ΔT is the difference between paleo and modern SSTs (T_m, 20.96°C), and b and c are empirical coefficients (-0.2 and 0.37, correspondingly). The differences between the records produced by the two approaches (+0.45 to -0.01‰SSS) are encouragingly low and lie within the standard error range of (7). Note the small deviation that applies to the salinity spike near 14.5 cal kyr B.P.

Conclusions

1. Isotopic sea surface temperature (SST) values that were estimated from $\delta^{18}O$ values of *G. ruber* (white) in modern sediments and *Levitus* [1982] salinity data were calibrated against various data sets of measured SST. The results show that the isotopic composition of *G. ruber* reflects most closely the

average water mass at 0-50 m water depth during summer ($r = 0.75$; equation (5)).

2. On the basis of Levitus SST data (0-50 m) for summer and $\delta^{18}O$ values *G. ruber* of modern sediments, a new transfer equation (8) was developed to estimate past local sea surface salinity values in the low-latitude Atlantic. These values generally match the *Levitus* [1982] SSS data (0-50 m) with $r = 0.81$ and a standard error of ±0.72 - ±0.77‰. The new transfer equation is particularly important for estimating the continental paleo runoff and the atmospheric water cycle in low latitudes from marine sediment cores.

3. The new equation was employed to tentatively reconstruct east Atlantic paleo salinity changes off the northwest Sahara where today continental runoff is absent and upwelled highly saline North Atlantic Central Water increases the local SSS in the Canary Current. During the LGM and large parts of Termination I the local SSS increased by 0.3-1.35‰, suggesting a general increase in the upwelling of highly saline NACW. Precisely coeval with Heinrich meltwater events 1 and 2, the upwelling broke down completely as recorded by short lasting salinity lows (36.1-37.0‰), possibly also induced by meltwater advection in the Canary Current from the north. Subsequently, major salinity spikes that are linked to SST maxima may reflect an evaporation maximum in the subtropical North Atlantic, the restoration of the Atlantic salinity conveyor belt, and a minimum in the Canary Current advection. The early Holocene salinity minimum near 9.0-5.5 ka reflects a strong continental runoff linked to the outstanding phase of north Saharan humidity during this time.

Acknowledgements. This research was supported by Alexander von Humboldt Foundation, DFG (Leibniz fund), the German National Climate Program, and the EC Environment Program. We thank Mark Maslin and Martin Trauth for helpful discussions, Hartmut Schulz for aid in data processing, Kyaw Winn for providing unpublished data (see Table 1), and Ulrike Hufnagel for preparing some of the $\delta^{18}O$ samples from the Gulf of Guinea. The helpful comments of Ken Miller and other reviewers are gratefully acknowledged.

References

Alley, R. B., et al., Abrupt increase in Greenland snow accumulation at the end of the Younger Dryas event, *Nature, 362*, 527-529, 1993.

Bainbridge, A. E., *Atlantic Expedition*, Vol. 2, *Section and Profiles*, 198 pp., U.S. Government Printing Office, Washington, D.C., 1981.

Bard, E., B. Hamelin, and R. G. Fairbanks, U-Th ages obtained by mass spectrometry in corals from Barbados: sea level during the past 130,000 years, *Nature, 346*, 456-458, 1990.

Bijma, J., W. W. Faber Jr., and C. Hemleben, Temperature and salinity limits for growth and survival of some planktonic foraminifers in Laboratory cultures, *J. Foraminiferal Res., 20*, 95-116, 1990.

Bond, G., et al., Evidence for massive discharges of icebergs into the North Atlantic Ocean during the last glacial period, *Nature, 360*, 245-249, 1992.

Bond, G., W. S. Broecker, S. Johnsen, J. McManus, L. Labeyrie, J. Jouzel, and G. Bonani, Correlations between climate records from North Atlantic sediments and Greenland ice, *Nature, 365*, 143-147, 1993.

Climate: Long-Range Investigation, Mapping, and Prediction (CLIMAP) Project Members, *Seasonal Reconstructions of the Earth's Surface at the Last Glacial Maximum*, Geological Society of America, Boulder, CO., 1981.

Craig, H and L. I. Gordon, Deuterium and oxygen-18 variations in the ocean and the marine atmosphere, in *Stable Isotopes in Oceanographic Studies and Paleotemperatures*, edited by E. Tongiorgi, pp. 9-130, Third SPOLETO conference on Nuclear Geology, Consiglio Nazionale delle Richerche, Laboratoria di Geologica Nucleare, Pisa, Italy, 1965.

Davis, J. C., *Statistics and Data Analysis in Geology*, pp. 201-204, John Wiley, New York, 1986.

Deuser, W. G., Seasonal variations in isotopic composition and deep-water fluxes of the test of perennially abundant planktonic foraminifera of the Sargasso Sea: Results from sediment-trap collections and their paleoceanographic significance. *J. Foraminiferal Res., 17*, 14-27, 1987.

Duplessy, J. C., Isotope studies, in *Climatic Change*, edited by J. Gribbin, pp. 46-67, Cambridge University Press, New York, 1978.

Duplessy, J.-C., L. Labeyrie, A. Juillet-Leclerc, F. Maitre, D. Josette, and M. Sarnthein, Surface salinity reconstruction of the North Atlantic during the last glacial maximum, *Oceanol. Acta, 14*, 311-324, 1991.

Duplessy, J. C., G. Delibrias, J. Turon, C. Pujol, and J. Duprat, Deglacial warming of the northeastern Atlantic Ocean: Correlation with the paleoclimatic evolution of the European continent, *Palaeogeogr. Palaeoclimatol. Palaeoecol., 35*, 121-144, 1981.

Duplessy, J. C., E. Bard, L. Labeyrie, J. Duprat, and J. Moyes, Oxygen isotope records and salinity changes in the northeastern Atlantic Ocean during the last 18,000 years, *Paleoceanography., 8*, 341-350, 1993.

Emiliani, C., Pleistocene temperatures, *J. Geol., 63*, 538-578, 1955.

Fairbanks, R. G., A 17,000-year glacio-eustatic sea level record: Influence of glacial melting rates on the Younger Dryas event and deep-ocean circulation, *Nature, 342*, 637-642, 1989.

Fairbanks, R. G., The age and origin of the "Younger Dryas climate event" in Greenland ice cores, *Paleoceanography, 5*, 937-948, 1990.

Fairbanks, R. G., and R. K. Matthews, The marine oxygen isotope record in Pleistocene coral, Barbados, West Indies, *Quat. Res., 10*, 181-196, 1978.

Fairbanks, R. G., M. Sverdlove, R. Free, P. H. Wiebe, and A. W. H. Bé, Vertical distribution and isotopic fractionation of living planktonic foraminifera from the Panama Basin, *Nature, 298*, 841-844, 1982.

Flower, B. P., and J. P. Kennett, The Younger Dryas cool episode in the Gulf of Mexico, *Paleoceanography, 5*, 949-961, 1990.

Ganssen, G., The record of coastal upwelling in stable isotopes of modern foraminifera off Northwest Africa (in German with English abstract), *Meteor Forschungsergeb. Reihe C, 37*, 1-46, 1983.

Geochemical Ocean Sections Study (GEOSECS) Excutive Committee, *GEOSECS Atlantic, Pacific, and Indian Ocean Expeditions, Shorebased Data and Graphics*, Vol. 7, edited by H. G. Ostlund, H. Craig, W. S. Broecker and D. Spencer, International Decade of Ocean Exploration, National Science Foundation, Washington, D.C., 1987.

Hartung, J., Fehlerfortpflanzung, in *Statistik, Lehr- und Handbuch der angewandten Statistik*, pp. 326-332, R. Oldenbourg, Munich, Germany, 1989.

Hemleben, C., M. Spindler, and O. R. Anderson, *Modern Planktonic Foraminifera*, 363 pp., Springer-Verlag, New York, 1989.

Hommers, H., Riesenkörner in Staubsedimenten von zwei Tiefseekernen vor Senegal, NW-Afrika (18°N, 18°W), M. sc. thesis, Univ. of Kiel, Kiel, Germany, 1989.

Hooghiemstra, H., A. Bechler, and H.-J. Beug, Isopollen maps for 18,000 years B.P. of the Atlantic offshore of northwest Africa: Evidence for paleowind circulation, *Paleoceanography, 2*, 561-582, 1987.

Imbrie, J., and N. G. Kipp, A new micropaleontological method for quatitative paleoclimatology: application to a late Pleistocene Caribbean core, in *The Late Cenozoic Glacial Ages*, edited by K. K. Turekian, pp. 71-181, Yale Univ. Press, New Haven, Ct, 1971

Jung, S., Zur Herkunft der Karbonate in Tiefseesedimenten des subtropischen und tropischen Ostatlantiks, Diploma thesis, 65 pp., Univ. of Kiel, Kiel, Germany, 1990.

Keigwin, L. D., and G. A. Jones, Glacial-Holocene stratigraphy,

chronology and paleoceanographic observations on some North Atlantic sediment drift, *Deep Sea Res., Part A, 36*, 845-867, 1989.

Kolesnikov, A. G., Equalant I and II Oceanographic Atlas, Vol. 1 Physical Oceanography, 100 pp., UNESCO, Paris, 1973.

Koopmann, B., Sedimentation von Saharastaub im subtropischen Nordatlantik während der letzten 25,000 Jahre, *Meteor Forschungsergeb. Reihe C, 35*, 23-59, 1981.

Labeyrie, L. D., J. C. Duplessy, and P. L. Blanc, Variations in mode of formation and temperature of oceanic deep waters over the past 125,000 years, *Nature, 327*, 477-482, 1987.

Levitus, S., *Climatological Atlas of the World Ocean*, 173 pp., U. S. Depart-ment of Commerce, National Oceanic and Atmospheric Administration, Silverspring, Md., 1982.

Lutze, G. F., M. Sarnthein, B. Koopmann, U. Pflaumann, H. Erlenkeuser, and J. Thiede, Meteor Cores 12309-2: Late Pleistocene reference section for interpretation of the Neogene of Site 397, edited by U. von Rad et al., *Initial Rep. Deep Sea Drilling Proj., 47, part 1*, 727-739, 1979.

Mix, A. C., and W. F. Ruddiman, Structure and timing of the last deglaciation: Oxygen-isotope evidence, *Quat. Sci. Rev., 4*, 59-108, 1985.

Mix, A. C., W. F. Ruddiman, and A. McIntyre, Late Quaternary paleoceanography of the tropical Atlantic, 2, The seasonal cycle of sea surface temperatures, 0-20,000 years B.P., *Paleoceanography, 1*, 339-353, 1986.

Molfino, B. E., Statistical modeling in paleoceanography; Paleoestimation of upper water-mass dynamics using marine microfossils, Ph D. Thesis, Brown Univ., Providence, R. I., 1993

O'Neil, J. R., R. N. Clayton, and T. K. Mayeda, Oxygen isotope fractionation in divalent metal carbonates, *J. Chem. Phys. 51*, 5547-5558, 1969.

Petit-Maire, N., Holocene biogeographical variations along the northwestern African coast (28°-19°N). Paleoclimatic implications, in *Sahara and Surrounding Seas, Sediments and Climatic Changes*, edited by M. Sarnthein et al., pp. 365-377, A. A. Balkema, Brookfield, Vt., 1980.

Petit-Maire, N. , Interglacial environments in presently hyperarid Sahara: Paleoclimatic implications, in *Paleoclimatology and Paleometerology: Modern and Past Patterns of Global Atmospheric Transport*, edited by M. Leinen and M. Sarnthein, pp. 637-661, Kluwer Academic Publishers, Boston, 1989

Pflaumann, U., Variations of the surface-water temperatures at the eastern North Atlantic continental margin (sediment surface samples, Holocene climatic optimum, and last glacial maximum), *Palaeoecol. Africa, 12*, 191-212, 1980.

Prentice, I. C., Biome modeling and the carbon cycle, in *The Global Carbon Cycle, NATO ASI Ser. I*, edited by M. Heimann, pp. 219-238, Springer-Verlag, Berlin, 1992

Ritchie, J. C., and C. V. Haynes, Holocene vegetation zonation in the eastern Sahara, *Nature, 304*, 645-647, 1987.

Rossignol-Strick, M., and D. Duzer, Late Quaternary pollen and dinoflagellate cysts in marine cores off West Africa, *Meteor Forschungsergeb., Reihe C*, 1-14, 1979.

Rosteck, F., G. Ruhland, F. C. Bassinot, P. J. Müller, L. D. Labeyrie, Y. Lancelot, and E. Bard, Reconstructing sea surface temperature and salinity using $\delta^{18}O$ and alkenone records, *Nature, 364*, 319-321, 1993.

Sarnthein, M., Sand deserts during glacial maximum and climatic optimum, *Nature, 272*, 43-46, 1978.

Sarnthein, M., Zur Fluktuation der subtropischen Wüstengürtel seit dem letzten Hochglazial vor 18.000 Jahren: Klimahinweise und -modelle aus Tiefseesedimenten, *Geomethodica, 7*, 125-161, 1982

Sarnthein, M., H. Erlenkeuser, and R. Zahn, The response of continental climate in the subtropics as recorded in deep-sea sediments., *Actes Colloq. Int. CNRS. Bordeaux, 31*, 393-407, 1982a.

Sarnthein, M., J. Thiede, U. Pflaumann, H. Erlenkeuser, D. Fütterer, B. Koopmann, H. Lange, and E. Seibold, Atmospheric and oceanic circulation patterns off northwest Africa during the past 25 million years, in *Geology of the Northwest African Continental Margin*, edited by U. von Rad et al., pp. 545-604, Springer-Verlag, New York, 1982b.

Sarnthein, M., E. Jansen, M. Arnold, J. C. Duplessy, H. Erlenkeuser, A. Flatoy, T. Veum, E. Vogelsang, and M. Weinelt, $\delta^{18}O$ time-slice reconstruction of meltwater anomalies at Termination I in the North Atlantic between 50 and 80°N, in *The Last Deglaciation: Absolute and Radiocarbon Chronologies*, edited by E. Bard and W. S. Broecker, pp. 183-200, Springer-Verlag, New York, 1992.

Sarnthein, M. , K. Winn, S. J. A. Jung, J. C. Duplessy, L. D. Labeyrie, H. Erlenkeuser, and G. Ganssen, Changes in east Atlantic deep water circulation over the last 30,000 years: Eight time slice reconstructions, *Paleoceano-graphy 9*, 209-267, 1994.

Schulz, H., Meeresoberflächentemperaturen im Nordatlantik und in der Norwegisch-Grönländischen See vor 9.000 Jahren. Auswirkungen des frühholozänen Insolationsmaximums, Ph. D. thesis Univ. of Kiel, Kiel Germany, 1994.

Shackleton, N. J., Attainment of isotopic equilibrium between ocean water and benthonic foraminifera genus *Uvigerina*: Isotopic changes in the ocean during the last glacial, in *Les Methodes quantitative detude des variations du climat au cours du Pleistocene, Colloq. Int. C.N.R.S., No. 219*, 203-209, 1974.

Shackleton, N. J., The oxygen isotope stratigraphic record of the late Pleistocene, *Phil. Trans. R. Soc. London. B., 208*, 169-182, 1977.

Slowey, N. C., and W. B. Curry, Structure of the glacial thermocline at Little Bahama Bank, *Nature, 328*, 55-58, 1987.

Street, F. A. and A. T. Grove, Global maps of lake-level fluctuation since 30,000 yr BP, *Quat. Res., 12*, 83-118, 1979.

Street-Perrott, F. A., D. S. Marchand, N. Roberts, and D. S. Harrison, Global Lake-Level Variations From 18,000 Years to 0 Years Ago: A Paleoclimatic Analysis, Oxford University Press, New York, 1989.

Thiede, J., Aspects of variability of the glacial and interglacial North Atlantic eastern boundary current (last 150,000 years), *Meteor Forschungsergeb. Reihe C*, 28, 1-36, 1977.

Tolderlund, D. S., and A. W. H. Bé, Seasonal distribution of planktonic foraminifera in the western North Atlantic, *Micropaleontology, 17*, 297-329, 1971.

Vogelsang, Paläo-Ozeanographie des Europäischen Nordmeeres an Hand stabiler Kohlenstoff- und Sauerstoffisotopen, Ph. D. thesis, 136 pp., Univ. of Kiel, Kiel, Germany, 1990

Williams, D. F., A. W. H. Bé, and R. G. Fairbanks, Seasonal stable isotopic variations in living planktonic foraminifera from Bermuda plankton tows, *Palaeogeogr. Palaeoclimatol. Palaeoecol., 33*, 71-102, 1981.

Winn, K., M. Sarnthein, and H. Erlenkeuser, $\delta^{18}O$ stratigraphy and chronology of Kiel sediment cores from the East Atlantic, *Ber. Rep. 45*, Geol. Paläontol. Inst. Univ. Kiel, Kiel, Germany, 1991.

Zahn-Knoll, R., Spätquartäre Entwicklung von Küstenauftrieb und Tiefen wasser zirkulation im Nordost- Atlantik. Reconstruktion anhand stabiler Isotopen kalkschaliger Foraminiferen (in German), Ph. D. thesis, Univ. of Kiel, Kiel, Germany, 1986.

J-C. Duplessy, Centre des Faibles Radioactivités, Laboratoire mixte CNRS-CEA, F-91198 Gif-sur-Yvette Cedex, France. (e-mail: duplessy@eole.cfr. cnrs-gif.fr)

H. Erlenkeuser, C^{14}-Labor, Institut für Reine und Angewandte Kernphysik, Universität Kiel, Olshausenstr. 40, D-24098 Kiel, Germany. (e-mail: pke47@rz.uni-kiel.d400.de)

S. Jung, U. Pflaumann, M. Sarnthein, L. Wang, Geologisch-Paläonto-logisches Institut, Universität Kiel, Olshausenstr. 40, D-24098 Kiel, Germany. (e-mail: sj@gpi.uni-kiel.de; up@gpi.uni-kiel.de; ms@gpi.uni-kiel.de; ljw@gpi.uni-kiel.de)

(Received August 2, 1994; revised February 14, 1995;
accepted February 14, 1995.)